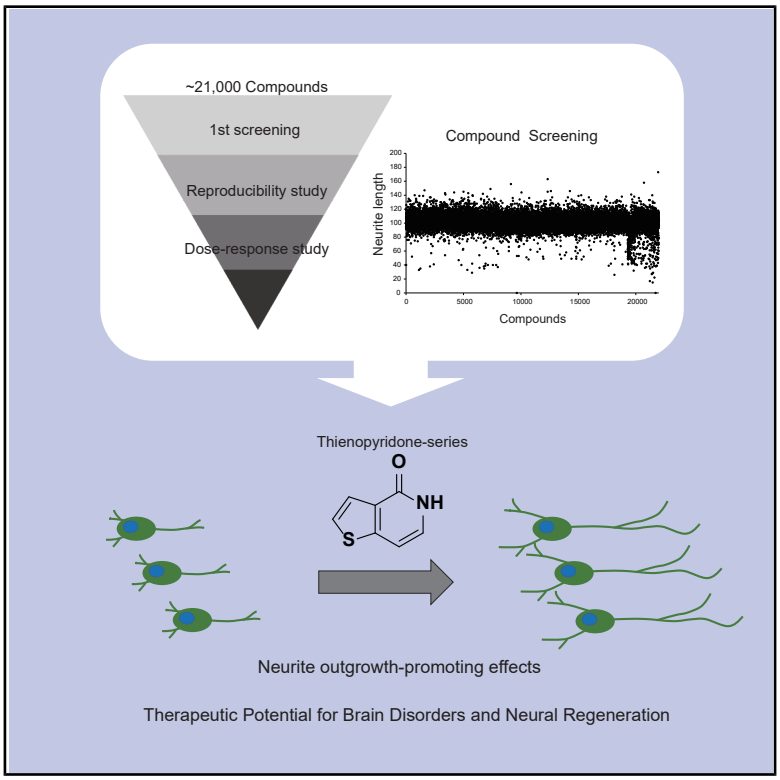
iScience

Article

Phenotypic screening of human iPSC-derived neurons identifies thienopyridones as neuritogenic small molecules

Graphical abstract



Authors

Keiko Imamura, Hiroshi Yukikate, Takeshi Hioki, ..., Yuko Arioka, Norio Ozaki, Haruhisa Inoue

Correspondence

haruhisa@cira.kyoto-u.ac.jp

In brief

Biological sciences; neuroscience; pharmacology; stem cells research

Highlights

- Phenotypic screening identifies neurite-promoting compounds in human iPSC-derived neurons
- Indazole hits identify TNIK as a kinase regulating neurite outgrowth
- Scaffold expansion reveals thienopyridone derivatives with neuritogenic activity
- Thienopyridones enhance neurite outgrowth in human neural organoids

Imamura et al., 2026, iScience *29*, 115529
May 15, 2026 © 2026 The Authors. Published by Elsevier Inc.
https://doi.org/10.1016/j.isci.2026.115529

CellPress

iScience

CellPress
OPEN ACCESS

Article

Phenotypic screening of human iPSC-derived neurons identifies thienopyridones as neuritogenic small molecules

Keiko Imamura,[1,2,3,4] Hiroshi Yukikate,[2,5] Takeshi Hioki,[2,6] Aya Okusa,[1,4] Keisuke Shibata,[2,5] Iñigo Narvaiza,[2,6] Akira Kaieda,[7] Bunnai Saito,[7] Nozomu Sakai,[7] Dang Ngoc Anh Suong,[1,3] Takeshi Niki,[1,3] Yuko Arioka,[8] Norio Ozaki,[8] and Haruhisa Inoue[1,2,3,4,9,*]

[1]Center for iPS Cell Research and Application (CiRA), Kyoto University, 53 Shogoin Kawahara-cho, Sakyo-ku, Kyoto 606-8507, Japan
[2]Takeda-CiRA (T-CiRA) Joint Program, 2-26-1, Muraoka-Higashi, Fujisawa 251-8555, Japan
[3]iPSC-based Drug Discovery and Development Team, RIKEN BioResource Research Center (BRC), 1-7 Hikaridai, Seika-cho, Soraku-gun, Kyoto 619-0237, Japan
[4]Medical-risk Avoidance Based on iPS Cells Team, RIKEN Center for Advanced Intelligence Project (AIP), 53 Shogoin Kawahara-cho, Sakyo-ku, Kyoto 606-8507, Japan
[5]Global Advanced Platform, Takeda Pharmaceutical Company Limited, 2-26-1, Muraoka-Higashi, Fujisawa 251-8555, Japan
[6]Neuroscience Drug Discovery Unit, Takeda Pharmaceutical Company Limited, 2-26-1, Muraoka-Higashi, Fujisawa 251-8555, Japan
[7]New Chemical Entity Production Laboratories, Takeda Pharmaceutical Company Limited, 2-26-1, Muraoka-Higashi, Fujisawa 251-8555, Japan
[8]Department of Psychiatry, Nagoya University Graduate School of Medicine, 65 Tsurumai-cho, Showa-ku, Nagoya 466-8550, Japan
[9]Lead contact
*Correspondence: haruhisa@cira.kyoto-u.ac.jp
https://doi.org/10.1016/j.isci.2026.115529

SUMMARY

Human induced pluripotent stem cell (iPSC)-derived neurons provide a platform for modeling brain disorders. Among disease-relevant cellular phenotypes, impaired neurite outgrowth has emerged as an indicator reflecting key aspects of neurological disease pathophysiology. We conducted a high-throughput phenotypic screening of over 21,000 small molecules to identify compounds that enhance neurite outgrowth in iPSC-derived neurons, and we identified three bioactive compounds sharing a common indazole scaffold. Notably, one of these compounds selectively targets TNIK, a kinase involved in neuronal development. Scaffold expansion led to the discovery of thienopyridone derivatives with potent neurite-promoting activity. Two thienopyridone compounds were further validated in a human neural organoid model, in which their neurite outgrowth-promoting effects were reproducibly confirmed. Transcriptomic profiling revealed activation of signaling pathways associated with neurotrophic stimulation. These findings identify thienopyridones as a scaffold for neuritogenic small molecules, suggesting their potential as a therapeutic strategy for brain disorders and for promoting neural regeneration.

INTRODUCTION

Recent advances in human induced pluripotent stem cell (iPSC) technology have enabled the generation of patient-derived neurons, providing an unprecedented platform for modeling the complex molecular mechanisms underlying neurological and psychiatric disorders.[1] Neurons differentiated from patient iPSCs are particularly valuable for elucidating disease-specific cellular phenotypes and for identifying therapeutic targets and candidate compounds.[2–5] Among the various cellular phenotypes, impaired neurite outgrowth—characterized as shortened or less elaborated neurites—has been frequently observed and is considered to mirror core aspects of disease pathology in the human brain. In neurodevelopmental disorders such as autism spectrum disorder (ASD), neurite outgrowth defects are thought to result from impaired synaptogenesis, disrupted neural circuit wiring, delayed neuronal maturation, and macroscopic structural abnormalities of the brain.[6–10] Similarly, in neurodegenerative diseases, neurite shortening is believed to reflect underlying processes such as axonal degeneration, cytoskeletal instability, mitochondrial dysfunction leading to energy deficits, and oxidative stress.[11,12] Thus, identifying small molecules capable of rescuing neurite outgrowth defects represents a crucial step toward both understanding disease mechanisms and developing therapeutic strategies for brain disorders.

In our previous work, we established disease models of neurodegenerative disorders by using iPSC-derived neurons, conducted large-scale compound screening, elucidated disease-specific cellular mechanisms, identified potential therapeutic targets, and progressed to clinical trials for promising compounds.[3,4] We consistently observed significant neurite shortening in patient-derived neurons modeling various

This is an open access article under the CC BY-NC-ND license (http://creativecommons.org/licenses/by-nc-nd/4.0/).

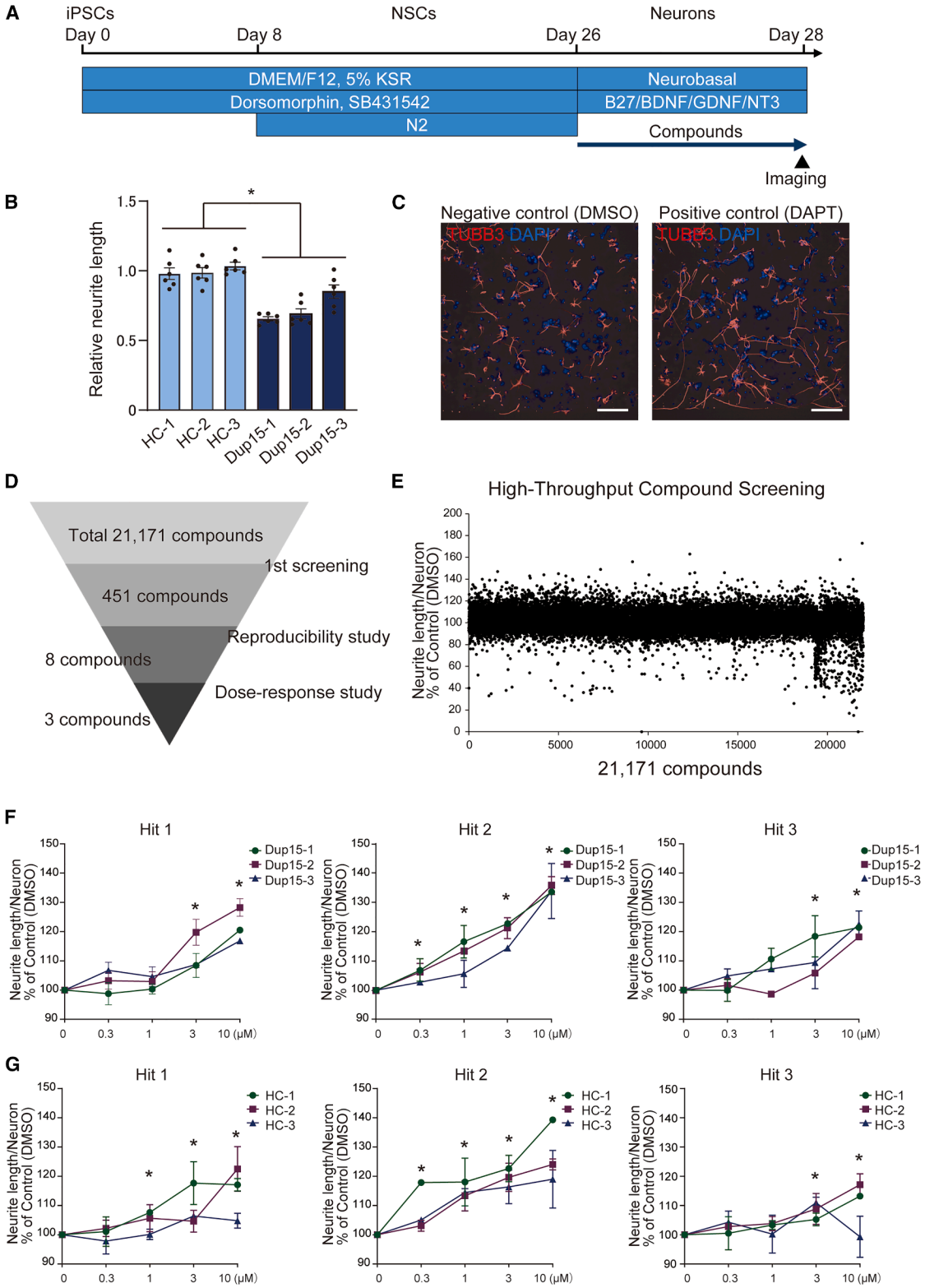


Figure 1. High-throughput screening for neurite outgrowth-promoting compounds

(A) Schedule for the generation of cortical neurons and compound screening.

(B) Comparison of neurite length between iPSC-derived neurons from healthy control (HCs) and patients with Dup15q syndrome. Neurite length per neuron was quantified in neurons derived from three independent HCs and three independent Dup15q syndrome (Dup15) iPSC lines to assess baseline differences for compound screening. Data were normalized to the mean value of HCs and are presented as the mean ± SEM. $n = 6$ wells per group. Student's t test, $^*p < 0.05$.

(legend continued on next page)

neurodegenerative diseases, reinforcing the relevance of this phenotype as an early marker of neurodegeneration. In the present study, we extended this approach to neurons derived from iPSCs of patients with hereditary forms of ASD, a disorder in which neurite shortening has also been reported *in vitro*.[13,14] Utilizing an extensive compound library comprising over 2.1 million molecules, including libraries annotated for target information and libraries enriched for diverse chemical scaffolds, we performed a comprehensive phenotypic screen. Through this effort, we identified chemical scaffolds that promote neurite outgrowth in human neurons, as well as associated binding proteins. Interestingly, the identified chemical scaffolds included not only known scaffolds previously implicated in promoting neurite growth but also new scaffolds. Binding proteins associated with the active compounds included molecules previously implicated in schizophrenia, intellectual disability, and ASD. Our findings, thus, provide new insights into the molecular control of neurite outgrowth and suggest therapeutic strategies for neurodevelopmental and neurodegenerative diseases.

RESULTS

High-throughput screening for neurite outgrowth-promoting compounds

We analyzed the cellular phenotypes associated with Dup15q syndrome, a chromosomal disorder caused by duplications of the 15q11–q13 region and associated with ASD. Cortical neurons were generated from iPSCs derived from three healthy control individuals and three patients with Dup15q syndrome (Tables S1 and S2), and their cellular phenotypes were examined. Cortical neurons were differentiated from human iPSCs, using a previously reported two-dimensional culture method[15] (Figure 1A). Cortical neurons derived from patients with Dup15q syndrome exhibited significantly shorter neurite length than those derived from healthy controls (Figures 1B and S1). Using this cellular phenotype, high-throughput screening (HTS) was conducted to identify compounds that promote neurite outgrowth. Compounds were administered from day 26 to day 28 of differentiation in cortical neurons derived from the Dup15-1 iPSC line cultured in 384-well plates, followed by fixation and immunostaining with anti-βIII-tubulin antibody. Neurite length was quantified using high-content image analysis. Compounds were evaluated using DMSO (0.1% v/v, with no detectable toxicity) as a negative control and 10 μM DAPT, a γ-secretase inhibitor that suppresses Notch signaling and has been reported to promote neurite extension,[16] as a positive control (Figure 1C). In the HTS assay validation, the coefficient of variation (%CV) was 6.8 ± 1.2 for the negative control and 7.2 ± 2.2 for the positive control (Figures S2A and S2B). A total of 21,171 compounds were evaluated using a hierarchical screening strategy (Figure 1D), followed by primary screening (Figure 1E). For compound screening, 19,200 compounds from a central nervous system (CNS)-focused library, 702 compounds from a kinase inhibitor library, and 1,269 compounds from an FDA-approved drug library were tested. Compounds from the CNS-focused library were screened at 10 μM, those from the kinase inhibitor library at 3 μM, and compounds from the FDA-approved drug library were screened at 3 and 10 μM. 1st screening was performed with a single replicate (n = 1 well), and compounds exhibiting responses greater than the mean plus three standard deviations (mean +3 SD) of the DMSO control were defined as active. This screening identified 409 (2.1%) compounds from the CNS-focused library, 10 (1.4%) compounds from the kinase inhibitor library, and 32 (2.5%) compounds from the FDA-approved drug library (Table S3). To evaluate reproducibility, 2nd screening (reproducibility study) was conducted with seven replicates (n = 7 wells). In this screen, compounds with responses exceeding the mean plus two standard deviations (mean +2 SD) of the DMSO control were classified as active. As a result, four compounds from the CNS-focused library, three from the kinase inhibitor library, and one from the FDA-approved drug library were identified, yielding a total of eight reproducible candidates (Table S4 and Figure S3). Among these, three compounds exhibited clear dose-dependent effects in cortical neurons derived from iPSCs of three patients with Dup15q syndrome (Figure 1F) as well as those derived from three healthy controls (Figure 1G) and were, therefore, defined as hit compounds. Interestingly, all three active compounds shared a common scaffold, indazole. This scaffold resembles known ATP-pocket binding motifs, commonly associated with kinase inhibitors.

Target annotation

We evaluated structural analogs centered on the three hit compounds, demonstrating consistency of activity and structure-dependent effects. Among the three hit compounds, two were not annotated, while one (Hit 2) was annotated as targeting TNIK, Aurora B, and MINK kinases, based on available annotation information obtained from the compound libraries provided by the companies. Binding assays were performed to evaluate the interaction of these compounds with the annotated targets (Figure 2A). Compounds exhibiting strong binding affinity to TNIK consistently showed neurite outgrowth activity. Many kinase inhibitors exhibit multi-target activity, and among the compounds that promoted neurite outgrowth, several were found to target TNIK, MINK, and Aurora B. In these compounds, inhibitory activity against TNIK was generally the most potent, while some compounds also showed relatively strong activity against Aurora B. Accordingly, compounds with relatively high selectivity for TNIK or Aurora B were selected for further evaluation. TNIK inhibitors enhanced

(C) Representative images of iPSC-derived neurons (Dup15-1) treated with negative control (DMSO) or positive control (DAPT). Scale bars, 200 μm.
(D) Strategy for the identification of hit compounds.
(E) Results of the high-throughput compound screening (1st screening). Each dot represents the response to an individual compound.
(F) Dose-response effects of three hit compounds in Dup15 iPSC-derived neurons. Dose-response analyses were performed in neurons derived from three independent Dup15 iPSC lines. Data are presented as the mean ± SD (N = 3 iPSC lines, n = 3 independent experiments). Statistical significance was determined by repeated two-way ANOVA, followed by Dunnett's post hoc test ($p < 0.05$). Asterisks indicate significant differences compared with control (DMSO).
(G) Dose-response effects of three hit compounds in HC iPSC-derived neurons. Dose-response analyses were performed in neurons derived from three independent HC iPSC lines. Data are presented as the mean ± SD (N = 3 iPSC lines, n = 3 independent experiments). Statistical significance was determined by repeated two-way ANOVA, followed by Dunnett's post-hoc test ($p < 0.05$). Asterisks indicate significant differences compared with control (DMSO).

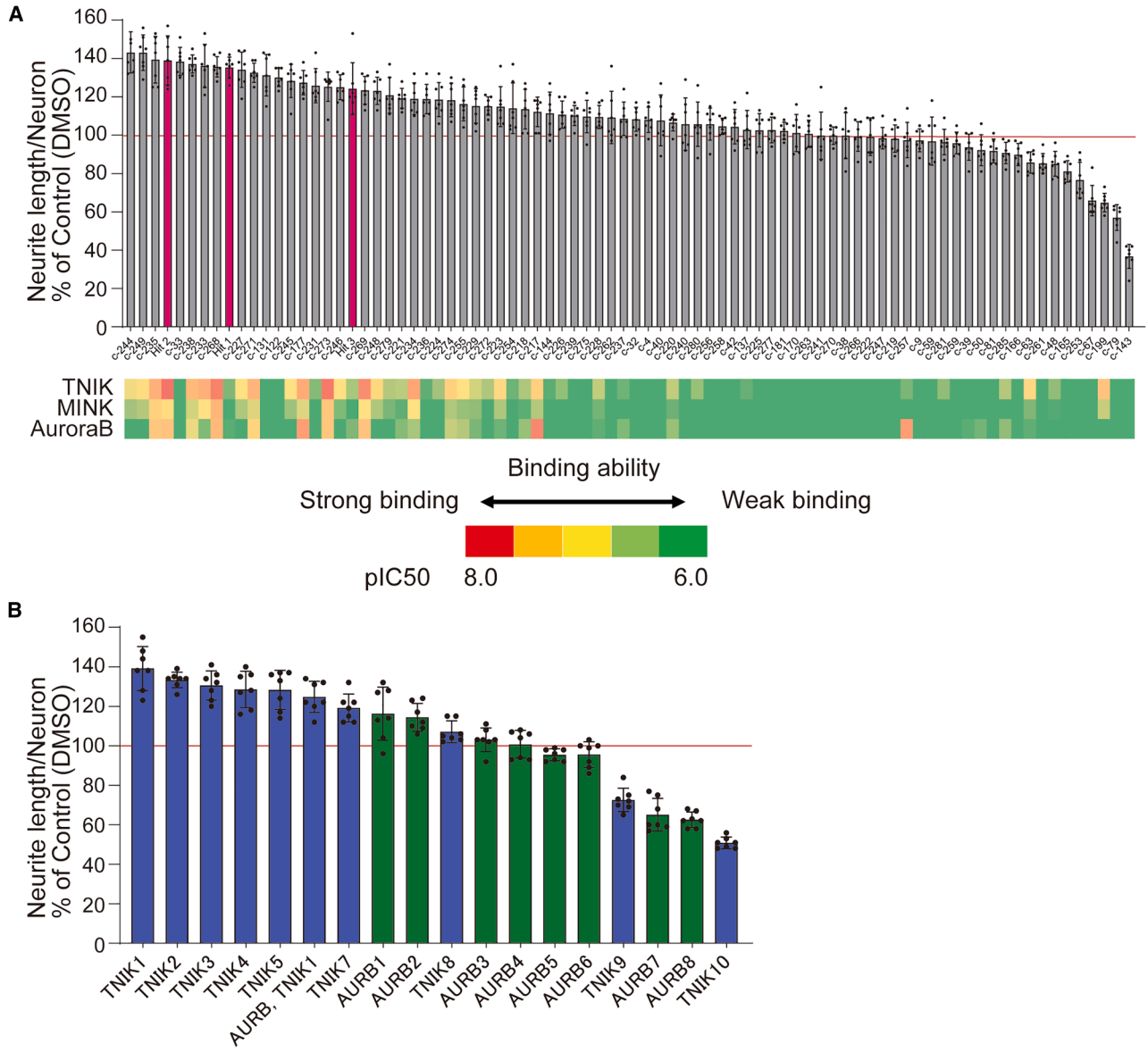


Figure 2. Mechanism of action study for neurite outgrowth

(A) Neurite extension and binding activity of active compounds toward TNIK, MINK, and Aurora B. Dup15-1 iPSC-derived neurons were treated with the indicated compounds at 10 μM for 2 days (n = 7 wells). Compounds showing strong binding activity to TNIK tended to promote neurite outgrowth. Magenta bars indicate data for the three hit compounds.

(B) Effects of TNIK inhibitors and Aurora B inhibitors on neurite outgrowth. Dup15-1 iPSC-derived neurons were treated with the indicated compounds at 10 μM for 2 days (n = 7 wells). TNIK inhibitors promoted neurite outgrowth. In contrast, Aurora B inhibitors did not show a clear enhancement of neurite outgrowth under the tested conditions. Blue bars indicate TNIK inhibitors, and green bars indicate Aurora B inhibitors.

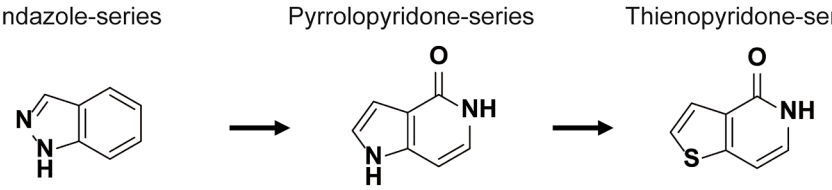
neurite outgrowth, whereas Aurora B inhibitors did not show a marked effect (Figure 2B). These results are consistent with previous reports[17] implicating TNIK in neurite extension, supporting the hypothesis that TNIK inhibition is a key mechanism underlying the observed neurite-promoting effect.

Scaffold expansion and derivative screening

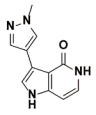
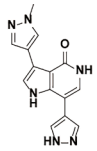
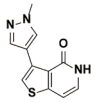
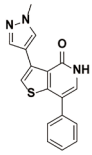
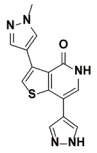
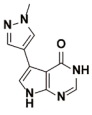
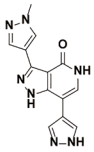
HTS identifies active hits, but the most potent hit is often unsuitable as a drug due to poor selectivity, drug-like properties, or safety liabilities; therefore, structure-activity relationship (SAR) analysis is essential to optimize potency together with druggability and to select compounds that can be developed into viable therapeutic candidates.

Because all three hit compounds shared a common indazole scaffold, structural modifications were introduced to this scaffold to further explore the chemical space. Figure 3A summarizes the scaffold-hopping strategy employed during the SAR campaign, in which systematic structural modifications of hit

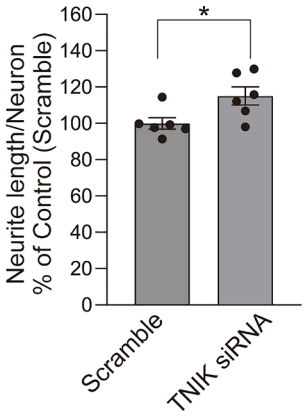
A



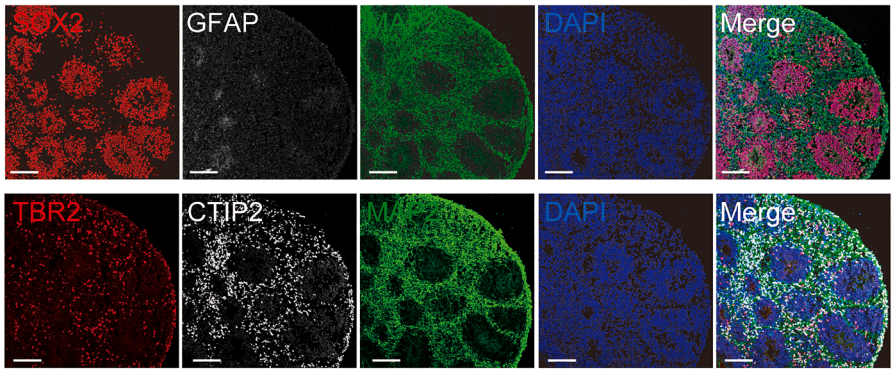
B

	Pyrrolopyridone scaffold		Thienopyridone scaffold			Pyrrolopyrimidone scaffold	Pyrazolopyridone scaffold
Chemical formula							
Compound ID	Compound A	Compound B	Compound C	Compound D	Compound E	Compound F	Compound G
0.3 uM	104	94.7	105.5	110.4	114.2	109	98.1
1 uM	105.7	96	108.6	120.3	133.2	106.9	98.8
3 uM	109.9	104	120.8	133.7	149.1	110.1	96.4
10 uM	123.5	94.1	131.3	149.3	143.8	100.2	100.6

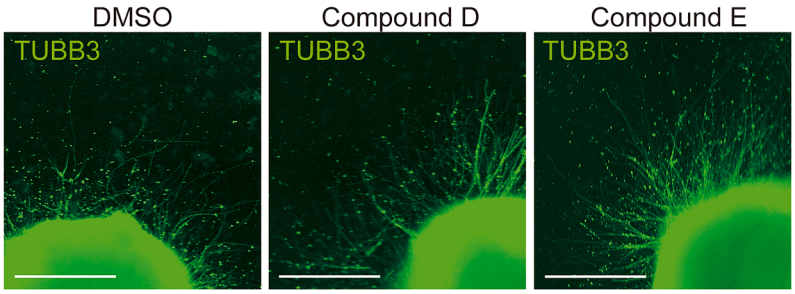
C



D



E



F

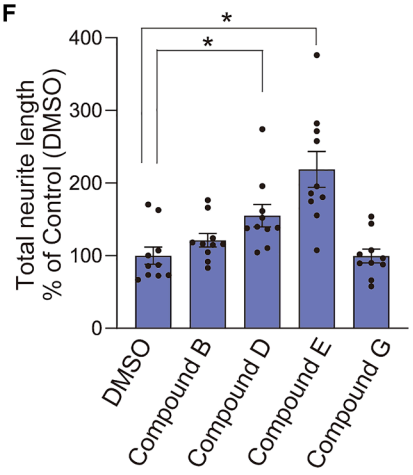


Figure 3. Scaffold expansion and derivative screening

(A) Structural expansion based on structure-activity relationship (SAR) study. Based on the indazole scaffold, structural expansion was performed guided by SAR analysis.

(legend continued on next page)

compounds were explored to evaluate how changes in the chemical scaffold affect biological activity and to guide lead optimization.[18] Scaffold hopping was performed to identify alternative core structures while maintaining key pharmacophoric features, thereby improving potency and drug-like properties.[19] Specifically, the initial indazole hit scaffold was expanded to related bicyclic chemotypes, including the pyrrolopyridone and thienopyridone series (Figure 3A). In the initial SAR studies, a variety of substituents were introduced at different positions in the indazole series.

The SAR of seven representative compounds is summarized in Figure 3B. These compounds were evaluated at four concentrations (0.3, 1, 3, and 10 μM) in Dup15-1 neurons. Compounds were classified as active when the measured value exceeded the mean +2 SD of the DMSO control, and they were classified as inactive when the value was below this threshold. Among the scaffolds examined, compound A (pyrrolopyridone scaffold) and compound C (thienopyridone scaffold), both containing a pyridone ring within the bicyclic system, exhibited a clear concentration-dependent increase in activity. Because compound C (thienopyridone scaffold) showed more promising activity than compound A (pyrrolopyridone scaffold), various substituents were introduced at the 7-position of the thienopyridone scaffold. As a result, compound D, bearing a phenyl group, and compound E, bearing a pyrazole group at the 7-position, demonstrated higher potency than the unsubstituted compound C. In contrast, introduction of a pyrazole group at the 7-position of compound A (pyrrolopyridone scaffold) afforded compound B, which exhibited only weak activity, even at 10 μM, and was markedly less active than compound E. In addition, related bicyclic scaffolds—compound G (pyrazolopyridone scaffold) and compound F (pyrrolopyrimidone scaffold)—were found to be inactive. Taken together, these results highlighted the thienopyridone scaffold as the most promising scaffold.

Collectively, these results indicate that the thienopyridone scaffold plays a critical role in activity enhancement and that the incorporation of an aromatic moiety, such as a phenyl or pyrazole group, into the thienopyridone scaffold substantially increases potency. No hits bearing the monocyclic pyridone scaffold including 2-pyridone, as described in previous reports,[20] were obtained in this study. To confirm these findings, we also verified that thienopyridone compounds promote neurite outgrowth in neurons derived from a healthy control iPSC line (Figure S4). A kinase assay demonstrated that thienopyridone compounds exhibit inhibitory activity against TRAF2 and NCK-interacting kinase (TNIK). In a Time-Resolved Fluorescence Resonance Energy Transfer (TR-FRET)-based kinase profiling assay, TNIK inhibition by compound E was directly quantified, showing 86.1% inhibition at 0.1 μM and 99.9% inhibition at 1 μM, corresponding to a pIC50 value of 7.80. In addition, knockdown of TNIK by siRNA was shown to induce neurite outgrowth (Figure 3C). Based on these observations, it was inferred that thienopyridones promote neurite outgrowth through inhibition of TNIK. However, this evidence is indirect, and given the non-selective activity profiles of these compounds, the involvement of alternative mechanisms in mediating neurite outgrowth cannot be excluded.

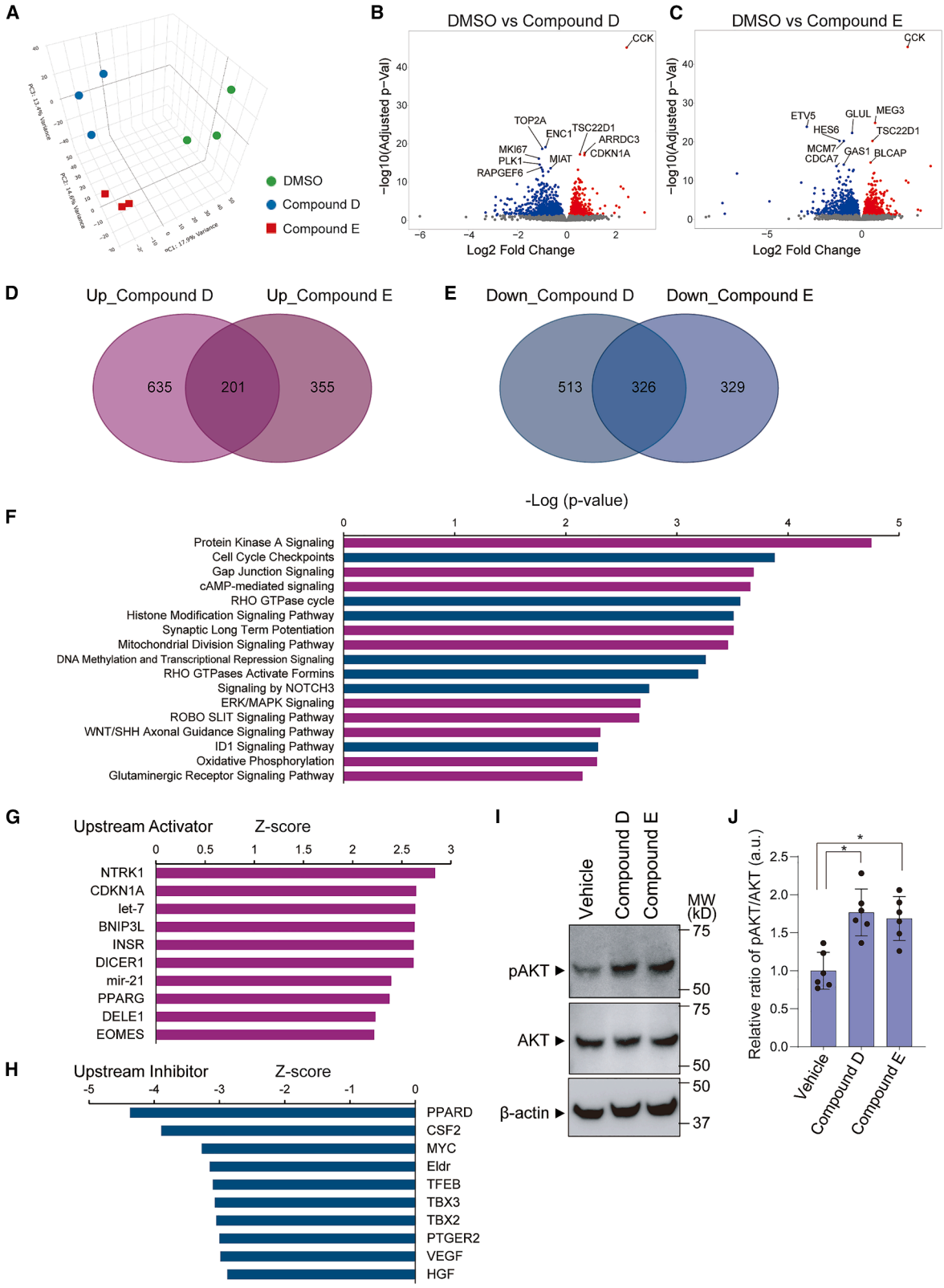
Neural organoid-based validation

Two compounds with the thienopyridone scaffold that exhibited strong activity in a two-dimensional culture were further evaluated using human iPSC-derived neural organoids. Organoids were generated from healthy control iPSCs (HC-4) and transferred onto iMatrix-coated plates at day 30 (Figure 3D), followed by two weeks of compound treatment. Organoids adhered to the plates and extended neurites,[21–23] and the total length of neurites extending from each individual organoid was quantitatively analyzed. Both thienopyridone compounds successfully reproduced the neurite outgrowth phenotype in the organoid model, which confirmed their efficacy in neural organoids (Figures 3E and 3F). While this phenotype is interpreted primarily as neurite outgrowth, contributions from general tissue outgrowth or cell movement in the three-dimensional organoid context cannot be entirely excluded.

Transcriptomic profiling and pathway analysis

To elucidate the molecular mechanisms underlying the activity of the two thienopyridone compounds, RNA sequencing was performed on organoids (HC-4) treated with the thienopyridone compounds D and E, each administered at 3 μM for 3 days. Each compound induced distinct changes in gene expression (Figures 4A–4C), and several genes implicated in neuronal differentiation and morphological remodeling, such as *CDKN1A*, *MEG3*, and *CCK*, were found to be upregulated. In total, 201 genes were concordantly upregulated (Figure 4D), whereas 326 genes were concordantly downregulated in organoids treated with both compound D and compound E (Figure 4E). Pathway analysis using these upregulated and downregulated gene sets identified the enrichment of pathways associated with neurite outgrowth, including protein kinase A signaling, Robo-Slit signaling, and axonal guidance signaling (Figure 4F). Furthermore, upstream regulator analysis was performed to identify putative upstream activators (Figure 4G) and inhibitors (Figure 4H), which revealed NTRK1 as a predicted upstream activator (Figure 4G). On the basis of these results, we performed western blot analysis to examine AKT, a downstream effector of this pathway, and observed that the treatment with thienopyridones increased the levels of phosphorylated AKT (Figures 4I

(B) Screening of derivative compounds in Dup15 iPSC-derived neurons. Neurite outgrowth rates (% relative to DMSO) are summarized in the table. Values exceeding 2 standard deviations (+2 SD) above the DMSO mean are indicated in blue.
(C) Effect of TNIK siRNA on neurite outgrowth. TNIK siRNA treatment promoted neurite outgrowth compared with scramble siRNA control. Data are presented as the mean ± SEM ($n = 6$ wells). Statistical significance was assessed using Student's t test. $^{*}p < 0.05$.
(D) Representative immunofluorescence images of neuronal organoids at day 30, showing the expression of cortical neuron markers. Scale bars, 100 μm.
(E) Neurite outgrowth of neural organoids. Compound D and compound E showed neurite outgrowth of neural organoids. Scale bars, 500 μm.
(F) Quantitative analysis of neurite outgrowth of neural organoids. Compound D and compound E showed neurite outgrowth of neural organoids. $n = 10$ organoids, mean ± SE, one-way ANOVA, $p < 0.05$; post hoc test, $^{*}p < 0.05$).



(legend on next page)

and 4J). Given that AKT is a well-established regulator of neurite outgrowth, these data suggest that the activation of AKT signaling downstream of NTRK1 and the modulation of neurotrophic signaling pathways[24,25] may contribute to the neurite outgrowth-promoting effects of thienopyridone compounds observed in this study.

DISCUSSION

In this study, we conducted large-scale compound screening by using human iPSC-derived neurons, and we evaluated more than 21,000 small molecules. Through this screening, we identified compounds capable of promoting neurite outgrowth with TNIK inhibition. Subsequent SAR studies revealed that compounds with a thienopyridone core exhibited particularly potent neurite-elongating effects. Further mechanistic analysis suggested that thienopyridone compounds activate intracellular signaling pathways similar to those stimulated by neurotrophic factors.

The pyridone scaffold is a key heterocyclic motif found in numerous biologically active compounds, and it is particularly valuable within the fields of medicinal chemistry, pharmacology, and drug discovery.[26] Structurally, it consists of a pyridine ring bearing a keto group and forms a lactam-type configuration. Among pyridone derivatives, 2-pyridones—six-membered nitrogen-containing heterocycles—have been widely studied for their broad spectrum of biological activities. These include anti-microbial, anti-malarial, anti-tumor, cardiotonic, and anti-fibrotic effects, as well as the promotion of neurite outgrowth, which highlight their versatility in modulating various biological processes.[26] In contrast, the thienopyridone scaffold investigated in this study consists of a fused heterocyclic system composed of a thiophene ring and a pyridone moiety. Thienopyridones are a class of compounds characterized by a thieno[2,3-*b*]pyridine or thieno[3,2-*c*]pyridine ring structure bearing a ketone functional group. Pharmacologically, they are primarily known as protein kinase inhibitors. Notably, some thienopyridones function as cyclin-dependent kinase (CDK) inhibitors involved in cell cycle regulation or as ATP-competitive inhibitors of casein kinase 2 (CK2), contributing anti-cancer and anti-inflammatory effects. In addition, several studies have reported their inhibitory activity against phosphatases of regenerating liver (PRLs),[27] as well as their selective activation of AMP-activated protein kinase (AMPK).[28,29] However, the effects of thienopyridones on neurons have not been extensively characterized.

Our results demonstrated that thienopyridones promote neurite outgrowth in human iPSC-derived neurons. Neurite shortening has been reported as a cellular phenotype in disease models using iPSC-derived neurons, particularly in studies of neurodevelopmental and neurodegenerative disorders. Therefore, compounds that can reverse neurite deficits may serve as therapeutic candidates for such diseases. Moreover, promoting neurite extension has important implications for neural regeneration. Because the mature CNS has limited regenerative capacity, the ability to regenerate neurites is the key to reconstructing lost neural circuits. Notably, thienopyridones exhibit higher lipophilicity than 2-pyridones, and this characteristic is expected to improve membrane permeability, as well as contribute to enhanced cellular uptake and increased penetration across the blood-brain barrier, suggesting that thienopyridone-based compounds possess the potential for broader applications within the CNS.

In conclusion, through large-scale screening of human iPSC-derived neurons, we identified thienopyridones as a class of small molecules that promote neurite outgrowth. These findings may contribute to the development of new therapeutic strategies in regenerative medicine and neurological disease treatment.

Limitations of the study

The findings are currently based solely on *in vitro* analyses using iPSC-derived neurons. Although we confirmed the robustness of the neurite-promoting effect in both two-dimensional neuronal cultures and three-dimensional neural organoids, iPSC-derived neurons remain immature compared with adult human neurons. Therefore, it remains to be determined whether thienopyridone compounds can promote neurite outgrowth in fully mature neurons *in vivo*. Nevertheless, considering recent advances in therapeutic strategies, these compounds may hold promise for enhancing therapeutic outcomes.

Figure 4. Transcriptomic analysis of neurite outgrowth induced by thienopyridones

(A) RNA-seq data from organoids treated with DMSO, compound D, or compound E; principal-component analysis (PCA) is presented.

(B) Volcano plot analysis of gene expression comparing DMSO and compound D. Gene names corresponding to the top 10 genes with the lowest p values are labeled in the plot.

(C) Volcano plot analysis of gene expression comparing DMSO and compound E. Gene names corresponding to the top 10 genes with the lowest p values are labeled in the plot.

(D) Venn diagram showing the overlap between genes upregulated by compound D and genes upregulated by compound E compared with DMSO (FDR < 0.05).

(E) Venn diagram showing the overlap between genes downregulated by compound D and genes downregulated by compound E compared with DMSO (FDR < 0.05).

(F) Pathway analysis of genes commonly differentially expressed in response to compound E and compound D. Magenta bars indicate pathways enriched among upregulated genes, and green bars indicate pathways enriched among downregulated genes.

(G) Predicted upstream activators of genes commonly differentially expressed by compound D and compound E.

(H) Predicted upstream repressors of genes commonly differentially expressed by compound D and compound E.

(I) Western blot analysis of AKT phosphorylation following compound treatment. iPSC-derived neurons at day 26 from the HC-4 line were treated with vehicle (DMSO), 3 μM compound D, or 3 μM compound E for 3 days. Treatment with either compound increased the level of phosphorylated AKT (pAKT).

(J) Quantification of pAKT:AKT ratio in iPSC-derived neurons. The pAKT:AKT ratio was quantified from six independent western blot experiments and normalized to the mean value of the vehicle control, which was set to 1. Data are presented as the mean ± SD (n = 6 independent experiments). Statistical significance was assessed by one-way ANOVA, followed by Dunnett's post hoc test. *p < 0.05.

RESOURCE AVAILABILITY

Lead contact

Further information, requests, or inquiries should be directed to and will be fulfilled by the lead contact, Haruhisa Inoue, haruhisa@cira.kyoto-u.ac.jp.

Materials availability

Materials will be available upon reasonable request and discussion.

Data and code availability

- RNA-seq data have been deposited in the NCBI Gene Expression Omnibus (GEO) under the accession number GEO: GSE308370 and are publicly available.
- Original code was not generated in this study.
- Any additional information required to reanalyze the data reported in this paper is available from the lead contact upon request

ACKNOWLEDGMENTS

We would like to express our sincere gratitude to all coworkers and collaborators: to Shinya Yamanaka and Yasushi Kajii for scientific discussions; and to Makoto Furusawa, Satoru Hayashi, Katsunori Sasa, Taeko Yoshida, Eri Ejiri, Misako Takemoto, and Yosuke Morizawa for their support. This work was supported by funding from the Japan Agency for Medical Research and Development (AMED) (grant numbers JP23bm1323001, JP22bm0804034, JP23bm1423014, JP24wm0625501, JP25bm1423029, JP24bm1123047, and JP24wm0625201), MHLW Intractable Diseases Program (Grant Number JPMH24FC1008), and Takeda Pharmaceutical Company Limited to H.I. and from AMED (grant number JP25wm0625518) to N.O.

AUTHOR CONTRIBUTIONS

Conceptualization and experimental design, H.I., H.Y., and K.I.; formal analysis, K.I., H.Y., T.H., A.O., K.S., I.N., A.K., B.S., N.S., D.N.A.S., and T.N.; material provision and analysis; Y.A. and N.O.; writing – original draft, K.I. and H.I.; writing – review & editing, K.I., H.Y., K.S., I.N., A.K., B.S., N.S., and H.I.

DECLARATION OF INTERESTS

H.Y., T.H., K.S., I.N., A.K., B.S., and N.S. are employees of Takeda Pharmaceutical Company Limited.

DECLARATION OF GENERATIVE AI AND AI-ASSISTED TECHNOLOGIES IN THE WRITING PROCESS

During the preparation of this work, the authors used ChatGPT (OpenAI, GPT-5) solely for English language editing and readability improvement. After using this tool, the authors reviewed and edited the content as needed and take full responsibility for the content of the publication.

STAR★METHODS

Detailed methods are provided in the online version of this paper and include the following:

- KEY RESOURCES TABLE
- EXPERIMENTAL MODEL AND STUDY PARTICIPANT DETAILS
- METHOD DETAILS
  - iPSC culture
  - Generation of cortical neurons from iPSCs
  - Generation of neural organoids
  - Immunocytochemistry and analysis of neurite outgrowth
  - TR-FRET-based kinase profiling assays
  - TNIK knockdown using siRNA
  - RNAseq analysis
  - Western blot analysis
- QUANTIFICATION AND STATISTICAL ANALYSIS

SUPPLEMENTAL INFORMATION

Supplemental information can be found online at https://doi.org/10.1016/j.isci.2026.115529.

Received: August 25, 2025
Revised: December 30, 2025
Accepted: March 26, 2026
Published: March 30, 2026

REFERENCES

1. Shi, Y., Inoue, H., Wu, J.C., and Yamanaka, S. (2017). Induced pluripotent stem cell technology: a decade of progress. Nat. Rev. Drug Discov. *16*, 115–130. https://doi.org/10.1038/nrd.2016.245.
2. Okano, H., and Morimoto, S. (2022). iPSC-based disease modeling and drug discovery in cardinal neurodegenerative disorders. Cell Stem Cell *29*, 189–208. https://doi.org/10.1016/j.stem.2022.01.007.
3. Imamura, K., Izumi, Y., Watanabe, A., Tsukita, K., Woltjen, K., Yamamoto, T., Hotta, A., Kondo, T., Kitaoka, S., Ohta, A., et al. (2017). The Src/c-Abl pathway is a potential therapeutic target in amyotrophic lateral sclerosis. Sci. Transl. Med. *9*, eaaf3962. https://doi.org/10.1126/scitranslmed.aaf3962.
4. Kondo, T., Imamura, K., Funayama, M., Tsukita, K., Miyake, M., Ohta, A., Woltjen, K., Nakagawa, M., Asada, T., Arai, T., et al. (2017). iPSC-Based Compound Screening and In Vitro Trials Identify a Synergistic Anti-amyloid β Combination for Alzheimer's Disease. Cell Rep. *21*, 2304–2312. https://doi.org/10.1016/j.celrep.2017.10.109.
5. Imamura, K., Nagahashi, A., Okusa, A., Sakasai, T., Tsukita, K., Kutoku, Y., Ohsawa, Y., Sunada, Y., Sahara, N., Kanaan, N.M., et al. (2025). iPSC screening identifies CACNA2D2 as a potential therapeutic target for FTLD-Tau. Eur. J. Cell Biol. *104*, 151484. https://doi.org/10.1016/j.ejcb.2025.151484.
6. Rao, S.R., Kostic, A., Baillargeon, P., Fernandez-Vega, V., de Anda, M.R., Fletcher, K., Shumate, J., Scampavia, L., Buxbaum, J.D., and Spicer, T.P. (2022). Screening for modulators of autism spectrum disorder using induced human neurons. SLAS Discov. *27*, 128–139. https://doi.org/10.1016/j.slasd.2022.01.004.
7. Sekiguchi, M., Sobue, A., Kushima, I., Wang, C., Arioka, Y., Kato, H., Kodama, A., Kubo, H., Ito, N., Sawahata, M., et al. (2020). ARHGAP10, which encodes Rho GTPase-activating protein 10, is a novel gene for schizophrenia risk. Transl. Psychiatry *10*, 247. https://doi.org/10.1038/s41398-020-00917-z.
8. Vadodaria, K.C., Ji, Y., Skime, M., Paquola, A.C., Nelson, T., Hall-Flavin, D., Heard, K.J., Fredlender, C., Deng, Y., Elkins, J., et al. (2019). Altered serotonergic circuitry in SSRI-resistant major depressive disorder patient-derived neurons. Mol. Psychiatry *24*, 808–818. https://doi.org/10.1038/s41380-019-0377-5.
9. Nakashima, H., Tsujimura, K., Irie, K., Ishizu, M., Pan, M., Kameda, T., and Nakashima, K. (2018). Canonical TGF-β Signaling Negatively Regulates Neuronal Morphogenesis through TGIF/Smad Complex-Mediated CRMP2 Suppression. J. Neurosci. *38*, 4791–4810. https://doi.org/10.1523/jneurosci.2423-17.2018.
10. Beltrão-Braga, P.C.B., and Muotri, A.R. (2017). Modeling autism spectrum disorders with human neurons. Brain Res. *1656*, 49–54. https://doi.org/10.1016/j.brainres.2016.01.057.
11. Fujimori, K., Ishikawa, M., Otomo, A., Atsuta, N., Nakamura, R., Akiyama, T., Hadano, S., Aoki, M., Saya, H., Sobue, G., and Okano, H. (2018). Modeling sporadic ALS in iPSC-derived motor neurons identifies a potential therapeutic agent. Nat. Med. *24*, 1579–1589. https://doi.org/10.1038/s41591-018-0140-5.
12. Egawa, N., Kitaoka, S., Tsukita, K., Naitoh, M., Takahashi, K., Yamamoto, T., Adachi, F., Kondo, T., Okita, K., Asaka, I., et al. (2012). Drug screening

for ALS using patient-specific induced pluripotent stem cells. Sci. Transl. Med. *4*, 145ra104. https://doi.org/10.1126/scitranslmed.3004052.

13. Deshpande, A., Yadav, S., Dao, D.Q., Wu, Z.Y., Hokanson, K.C., Cahill, M.K., Wiita, A.P., Jan, Y.N., Ullian, E.M., and Weiss, L.A. (2017). Cellular Phenotypes in Human iPSC-Derived Neurons from a Genetic Model of Autism Spectrum Disorder. Cell Rep. *21*, 2678–2687. https://doi.org/10.1016/j.celrep.2017.11.037.
14. Russo, F.B., Brito, A., de Freitas, A.M., Castanha, A., de Freitas, B.C., and Beltrão-Braga, P.C.B. (2019). The use of iPSC technology for modeling Autism Spectrum Disorders. Neurobiol. Dis. *130*, 104483. https://doi.org/10.1016/j.nbd.2019.104483.
15. Kondo, T., Asai, M., Tsukita, K., Kutoku, Y., Ohsawa, Y., Sunada, Y., Imamura, K., Egawa, N., Yahata, N., Okita, K., et al. (2013). Modeling Alzheimer's disease with iPSCs reveals stress phenotypes associated with intracellular Abeta and differential drug responsiveness. Cell Stem Cell *12*, 487–496. https://doi.org/10.1016/j.stem.2013.01.009.
16. Okubo, T., Nagoshi, N., Kohyama, J., Tsuji, O., Shinozaki, M., Shibata, S., Kase, Y., Matsumoto, M., Nakamura, M., and Okano, H. (2018). Treatment with a Gamma-Secretase Inhibitor Promotes Functional Recovery in Human iPSC- Derived Transplants for Chronic Spinal Cord Injury. Stem Cell Rep. *11*, 1416–1432. https://doi.org/10.1016/j.stemcr.2018.10.022.
17. Wu, X., Zhang, Z., Qiu, Z., Wu, X., Chen, J., Liu, L., Liu, X., Zhao, S., Yang, Y., and Zhao, Y. (2024). TNIK in disease: from molecular insights to therapeutic prospects. Apoptosis *29*, 1361–1376. https://doi.org/10.1007/s10495-024-01987-w.
18. Tong, W., Welsh, W.J., Shi, L., Fang, H., and Perkins, R. (2003). Structure-activity relationship approaches and applications. Environ. Toxicol. Chem. *22*, 1680–1695. https://doi.org/10.1897/01-198.
19. Fong, H., Wang, C., Knoferle, J., Walker, D., Balestra, M.E., Tong, L.M., Leung, L., Ring, K.L., Seeley, W.W., Karydas, A., et al. (2013). Genetic correction of tauopathy phenotypes in neurons derived from human induced pluripotent stem cells. Stem Cell Rep. *1*, 226–234. https://doi.org/10.1016/j.stemcr.2013.08.001.
20. Sangwan, S., Yadav, N., Kumar, R., Chauhan, S., Dhanda, V., Walia, P., and Duhan, A. (2022). A score years' update in the synthesis and biological evaluation of medicinally important 2-pyridones. Eur. J. Med. Chem. *232*, 114199. https://doi.org/10.1016/j.ejmech.2022.114199.
21. Clarke, K.E., Tams, D.M., Henderson, A.P., Roger, M.F., Whiting, A., and Przyborski, S.A. (2017). A robust and reproducible human pluripotent stem cell derived model of neurite outgrowth in a three-dimensional culture system and its application to study neurite inhibition. Neurochem. Int. *106*, 74–84. https://doi.org/10.1016/j.neuint.2016.12.009.
22. Kobolak, J., Teglasi, A., Bellak, T., Janstova, Z., Molnar, K., Zana, M., Bock, I., Laszlo, L., and Dinnyes, A. (2020). Human Induced Pluripotent Stem Cell-Derived 3D-Neurospheres are Suitable for Neurotoxicity Screening. Cells *9*, 1122. https://doi.org/10.3390/cells9051122.
23. Brüll, M., Geese, N., Celardo, I., Laumann, M., and Leist, M. (2024). Preparation of Viable Human Neurites for Neurobiological and Neurodegeneration Studies. Cells *13*, 242. https://doi.org/10.3390/cells13030242.
24. Park, J.H., Lee, S.B., Lee, K.H., and Ahn, J.Y. (2012). Nuclear Akt promotes neurite outgrowth in the early stage of neuritogenesis. BMB Rep. *45*, 521–525. https://doi.org/10.5483/bmbrep.2012.45.9.114.
25. Read, D.E., and Gorman, A.M. (2009). Involvement of Akt in neurite outgrowth. Cell. Mol. Life Sci. *66*, 2975–2984. https://doi.org/10.1007/s00018-009-0057-8.
26. Zhang, Y., and Pike, A. (2021). Pyridones in drug discovery: Recent advances. Bioorg. Med. Chem. Lett. *38*, 127849. https://doi.org/10.1016/j.bmcl.2021.127849.
27. Tasker, N.R., Rastelli, E.J., Burnett, J.C., Sharlow, E.R., Lazo, J.S., and Wipf, P. (2019). Tapping the therapeutic potential of protein tyrosine phosphatase 4A with small molecule inhibitors. Bioorg. Med. Chem. Lett. *29*, 2008–2015. https://doi.org/10.1016/j.bmcl.2019.06.048.
28. Dite, T.A., Ling, N.X.Y., Scott, J.W., Hoque, A., Galic, S., Parker, B.L., Ngoei, K.R.W., Langendorf, C.G., O'Brien, M.T., Kundu, M., et al. (2017). The autophagy initiator ULK1 sensitizes AMPK to allosteric drugs. Nat. Commun. *8*, 571. https://doi.org/10.1038/s41467-017-00628-y.
29. Vazquez-Martin, A., Vellon, L., Quirós, P.M., Cufí, S., Ruiz de Galarreta, E., Oliveras-Ferraros, C., Martin, A.G., Martin-Castillo, B., López-Otín, C., and Menendez, J.A. (2012). Activation of AMP-activated protein kinase (AMPK) provides a metabolic barrier to reprogramming somatic cells into stem cells. Cell Cycle *11*, 974–989. https://doi.org/10.4161/cc.11.5.19450.
30. Nakagawa, M., Taniguchi, Y., Senda, S., Takizawa, N., Ichisaka, T., Asano, K., Morizane, A., Doi, D., Takahashi, J., Nishizawa, M., et al. (2014). A novel efficient feeder-free culture system for the derivation of human induced pluripotent stem cells. Sci. Rep. *4*, 3594. https://doi.org/10.1038/srep03594.
31. Velasco, S., Kedaigle, A.J., Simmons, S.K., Nash, A., Rocha, M., Quadrato, G., Paulsen, B., Nguyen, L., Adiconis, X., Regev, A., et al. (2019). Individual brain organoids reproducibly form cell diversity of the human cerebral cortex. Nature *570*, 523–527. https://doi.org/10.1038/s41586-019-1289-x.
32. Hirozane, Y., Toyofuku, M., Yogo, T., Tanaka, Y., Sameshima, T., Miyahisa, I., and Yoshikawa, M. (2019). Structure-based rational design of staurosporine-based fluorescent probe with broad-ranging kinase affinity for kinase panel application. Bioorg. Med. Chem. Lett. *29*, 126641. https://doi.org/10.1016/j.bmcl.2019.126641.
33. Ge, S.X., Son, E.W., and Yao, R. (2018). iDEP: an integrated web application for differential expression and pathway analysis of RNA-Seq data. BMC Bioinf. *19*, 534. https://doi.org/10.1186/s12859-018-2486-6.

CellPress
OPEN ACCESS

STAR★METHODS

KEY RESOURCES TABLE

REAGENT or RESOURCE	SOURCE	IDENTIFIER
Antibodies		
anti-βIII-tubulin	Cell Signaling Technology	Cat#5568
anti-MAP2	Abcam	Cat#ab5392
anti-SOX2	R&D Systems	Cat#MAB2018
anti-GFAP	Abcam	Cat#ab4674
anti-TBR2	abcam	Cat#ab216870
anti-CTIP2	Abcam	Cat#ab18465
anti-phosphorylated AKT	Cell Signaling Technology	Cat#9271
anti-AKT	Cell Signaling Technology	Cat#9272
anti-β-actin	Sigma-Aldrich	Cat#A5441
Chemicals, peptides, and recombinant proteins		
StemFit AK02N	Ajinomoto	Cat#RCAK02N
iMatrix-511	TAKARA	Cat#892012
TrypLE Select Enzyme	Thermo Fisher Scientific	Cat#12563-011
Y-27632	Nacalai Tesque	Cat#08945-84
Accumax	Nacalai Tesque	Cat#17087-54
DMEM/Ham's F12	Thermo Fisher Scientific	Cat#11330-032
KnockOut Serum Replacement	Thermo Fisher Scientific	Cat#10828-028
MEM Non-Essential Amino Acids Solution	Thermo Fisher Scientific	Cat#11140-050
L-glutamine	Thermo Fisher Scientific	Cat#25030-081
2-mercaptoethanol	Sigma-Aldrich	Cat#21985-023
dorsomorphin	Sigma-Aldrich	Cat#P5499
SB431542	Cayman Chemical	Cat#13031
Matrigel	Corning	Cat#354230
Neurobasal Medium	Thermo Fisher Scientific	Cat#21103-049
B27 without Vitamin A	Thermo Fisher Scientific	Cat#12587010
Glutamax	Thermo Fisher Scientific	Cat#35050061
BDNF	Peprotech	Cat#450-02
GDNF	Peprotech	Cat#450-10
NT-3	Peprotech	Cat#450-03
Accutase	Innovative Cell Technologies	Cat#AT-104
Glasgow-MEM	Thermo Fisher Scientific	Cat#11710035
sodium pyruvate	Thermo Fisher Scientific	Cat#11360070
IWR1	Sigma-Aldrich	Cat#681669
Chemically Defined Lipid Concentrate	Thermo Fisher Scientific	Cat#11905031
Amphotericin B	Thermo Fisher Scientific	Cat#15290-026
penicillin/streptomycin	Thermo Fisher Scientific	Cat#15140-122
Deposited data		
Raw and analyzed data	This paper	GEO: GSE308370
Experimental models: Cell lines		
Human iPS cells	Kyoto university	HC1F
Human iPS cells	Kyoto university	HC3E
Human iPS cells	Kyoto university	HC6E
Human iPS cells	Kyoto university	201B7
Human iPS cells	Kyoto university	GM20562AEL10

(*Continued on next page*)

Continued		
REAGENT or RESOURCE	SOURCE	IDENTIFIER
Human iPS cells	Kyoto university	GM22571EL2
Human iPS cells	Nagoya University	NMI005_1-13
Oligonucleotides		
TNIK siRNA	Dharmacon	ID: E−004542-00
scrambled control siRNA	Dharmacon	ID: D-001910-10
Software and algorithms		
iDEP2.01	Ge, Son & Yao	https://bioinformatics.sdstate.edu/idep20/

EXPERIMENTAL MODEL AND STUDY PARTICIPANT DETAILS

The generation and use of human iPSCs were approved by the Ethics Committees of Kyoto University (Approved number: R0091). The use of human iPSCs for the experiments was approved by the Ethics Committees of Kyoto University (Approved number: R0091) and the Research Ethics Review Committee of Takeda. All methods were performed according to the approved guidelines. The data on human iPSCs used in the present study are shown in Table S1. All cell lines were authenticated by karyotyping and genetic characterization and tested negative for mycoplasma contamination.

METHOD DETAILS

iPSC culture

Human iPSCs were maintained with StemFit AK02N medium (Ajinomoto, Tokyo, Japan) on laminin (iMatrix-511; TAKARA, Kusatsu, Japan) -coated six-well culture plates at 37°C in a standard 5% CO_2 incubator.[30] For passages of cells, iPSC colonies were treated with TrypLE Select Enzyme (Thermo Fisher Scientific, Waltham, MA) at 37°C and dissociated into single cells. The single-cell iPSC suspension was plated at a density of 13,000 cells per well in StemFit medium with 10 μM Y-27632 Rock inhibitor (Nacalai Tesque, Kyoto, Japan). The medium was changed to StemFit without Y-27632 on the following day, and thereafter the medium was changed every 2 days.

Generation of cortical neurons from iPSCs

Cortical neurons were generated from human iPSCs by the modified method previously described.[15] iPSCs were dissociated into single cells using Accumax (Nacalai Tesque) and were quickly reaggregated in V-bottom 96-well plates for suspension culture (Sumitomo Bakelite Co., Ltd. Tokyo, Japan). Embryoid bodies (EB) were cultured in DFK5% medium (DMEM/Ham's F12 (Thermo Fisher Scientific) supplemented with 5% KnockOut Serum Replacement (KSR) (Thermo Fisher Scientific), MEM Non-Essential Amino Acids Solution (NEAA) (Thermo Fisher Scientific), L-glutamine (Sigma-Aldrich, St. Louis, MO, USA), 0.1% 2-mercaptoethanol (Sigma-Aldrich)) with 2 μM dorsomorphin (Chemdea LLC, Ridgewood, NJ, USA) and 10 μM SB431542 (Cayman Chemical, Ann Arbor, MI, USA) in a neural inductive stage (days 0–8). After neural induction, EB were transferred onto Matrigel (Corning Incorporated, Corning, NY)-coated 6-well culture plates and cultured in DFK10% (DMEM/Ham's F12 supplemented with 10% KSR, NEAA, L-glutamine, 0.1% 2-mercaptoethanol) supplemented with 1x N2 supplement (Thermo Fisher Scientific), 2 μM dorsomorphin, and 10 μM SB431542 in the patterning stage (days 8–24). On day 26, neural precursor cells were separated from the plate bottom using Accumax and cultured in Neurobasal Medium (Thermo Fisher Scientific) supplemented with 1x B27 without Vitamin A (Thermo Fisher Scientific), 1x Glutamax (Thermo Fisher Scientific), 10 ng/mL BDNF, 10 ng/mL GDNF and 10 ng/mL NT-3 on Matrigel-coated 96-well culture plates or 384-well culture plates with compounds. On day 28, cells were fixed with 4% PFA and analyzed.

Generation of neural organoids

Neural organoids of cerebral cortex were generated from healthy control iPSCs; 201B7[5] by the modified method previously described.[31] Briefly, iPSCs were dissociated by Accutase (Innovative Cell Technologies, Inc. San Diego, CA) at 37°C and suspended into cortical differentiation medium 1 (CDM1: consisting of Glasgow-MEM with 20% Knockout Serum replacement, 0.1 mM non-essential amino acids mix (NEAA), 1 mM sodium pyruvate, 0.1 mM 2-mercaptoethanol, 1% penicillin/streptomycin) supplemented with 3 μM IWR1, 5 μM SB431542 and 20 μM Y-27632, followed by reaggregation with 9,000–18,000 cells in ultra-low-cell-adhesion V-bottomed 96-well plates (Sumitomo Bakelite). The aggregates were cultured in CDM1 medium supplemented with 3 μM IWR1 and 5 μM SB431542 in 5% CO2 at 37°C for 18 days. Then, the floating aggregates were cultured in 60-mm culture dishes (Corning) under orbital agitation at 60 rpm in CDM2 (CDM2: DMEM/F12 medium (Thermo Fisher Scientific)), 2 mM Glutamax (Thermo Fisher Scientific), 1% N2 supplement (Thermo Fisher Scientific), 1% Chemically Defined Lipid Concentrate (Thermo Fisher Scientific), 0.25 μg/mL Amphotericin B, and 1% penicillin/streptomycin. On day 30, the organoids were transferred onto iMatrix-coated 96-well plates,

treated with 3 μM compounds, and half of the compound-containing medium was replaced every 3–4 days. After 14 days, cells were fixed in 4% paraformaldehyde, and neurite length was quantified.

Immunocytochemistry and analysis of neurite outgrowth

Cells cultured in two-dimensional conditions were fixed in 4% paraformaldehyde for 30 min at room temperature, washed with PBS, and permeabilized in PBS containing 0.2% Triton X-100 for 10 min at room temperature, followed by blocking for 30 min with Block Ace (Yukijirushi). After incubation with primary antibodies, anti-βIII-tubulin antibody (1:2,000, Cell Signaling Technology), overnight at 4°C, cells were washed three times with PBS and incubated with appropriate secondary antibodies for 1 h at room temperature. Stained cortical neurons were imaged using Opera Phenix (PerkinElmer), and neurite outgrowth rate was measured by Harmony High Content Imaging (PerkinElmer). Neurons were identified as cells containing a DAPI-positive nucleus surrounded by βIII-tubulin–positive cytoplasm. βIII-tubulin–positive processes extending from the neuronal cell body were recognized as neurites, and their lengths were measured using automated image analysis. For each neuron, the average neurite length was calculated, and the mean neurite length per neuron was subsequently determined on a per-well basis.

Neural organoids attached to a two-dimensional substrate and extending neurites were stained and imaged using IN CELL6500, and neurite outgrowth rate was measured by IN Cell Developer toolbox software 1.9 (GE Healthcare). The total length of neurites extending from each individual organoid was quantitatively analyzed. Neurite outgrowth values were normalized on a per-organoid basis by calculating the total neurite length per organoid within each well.

TR-FRET-based kinase profiling assays

TR-FRET-based competitive binding assays for approximately 300 kinases have been conducted by Axcelead Drug Discovery Partners (Fujisawa, Japan), as previously reported.[32] The binding assays were performed using 1536-well, white, flat-bottomed plates (Greiner Bio-One). Assay buffer comprised 50 mmol/L HEPES, 10 mmol/L MgCl2, 1 mmol/L EGTA, 0.1 mmol/L DTT, and 0.01% Brij-35. BODIPY- or Cy5-conjugated kinase inhibitors bound to a highly conserved ATP-binding pocket in kinases were used as a fluorescent probe Tested compounds were applied at 0.1 and 1 μM in competitive binding assays for approximately 300 recombinant protein kinases with an epitope tag, such as GST or His_6. The probe concentration was defined at the K_D value for each fluorescent labeled probe. TR-FRET fluorescent signals from a terbium-labeled anti GST-tag or His-tag antibody to the fluorescent-labeled probe were measured using an EnVision plate reader (PerkinElmer, Waltham, MA, USA) with laser excitation at 340 nm and emissions at 495 and 520 nm, and laser excitation at 337 nm and emissions at 615 and 665 nm for the Bodipy-conjugated probes and the Cy5-conjugated probes, respectively. Inhibition rates were calculated based on the signals the 0% and 100% inhibition samples in the absence and presence of the non-labeled compound, respectively, according to the following equation.

$$\%\text{inhibition} = (1 - (\text{Sample} - \text{LowControl}) / (\text{HighControl} - \text{LowControl})) * 100$$

pIC50 values are calculated by curve fitting using a four parameter logistic equation using XLfit (IDBS). Three of four parameters, the bottom plateau, the top plateau and the slope factor are fixed to 0, 100 and 1, respectively.

TNIK knockdown using siRNA

Small interfering RNAs (siRNAs) targeting human TNIK (ID: E−004542-00) and a non-targeting scrambled control siRNA (D-001910-10) were purchased from Dharmacon. iPSC-derived neurons were plated onto 96-well plates on day 26 of differentiation. On day 27, TNIK-targeting siRNA or scrambled control siRNA was added to the culture medium at a final concentration of 1 μM. Cells were fixed with 4% paraformaldehyde on day 29 and subsequently immunostained with βIII-tubulin for quantification of neurite length.

RNAseq analysis

RNA sequencing was performed using organoids generated from a healthy control iPSC line (HC-4). Ten organoids were plated per well in 24-well plates under adherent culture conditions. Organoids were treated with DMSO, Compound D, or Compound E at a final concentration of 3 μM, with three wells assigned to each condition ($n = 3$ wells). After 3 days of treatment, organoids were collected for RNA extraction. Total RNA was extracted using the miRNeasy Mini Kit (QIAGEN) following the manufacturer's protocol, and RNA quality was assessed with an Agilent 2100 Bioanalyzer (Agilent Technologies). Employing the Switching Mechanism at 5′ End of RNA Template (SMART) technology to add adapter sequences to both ends of the first-strand cDNA, full-length cDNA was synthesized using the SMART-Seq mRNA Kit (Takara Bio USA, Inc.), followed by PCR amplification using primers recognizing the adapter sequences. Subsequently, the double-stranded cDNA was fragmented and tagged at both ends through a tagmentation reaction using the Nextera XT DNA Library Prep Kit (Illumina Inc.), which applies transposon-mediated fragmentation and adapter insertion. Amplified libraries were generated using index primers (IDT for Illumina - DNA/RNA UD Indexes, Integrated DNA Technologies, Inc.). The pooled libraries were sequenced on the NovaSeq 6000 system with the NovaSeq 6000 S4 Reagent Kit v1.5 (Illumina Inc.), generating 2 × 150 bp paired-end reads. The raw sequencing data were converted to FASTQ format using dedicated software (bcl2fastq Conversion Software, Illumina). All procedures were performed following the manufacturer's manuals. The sequencing reads were mapped to the GRCh38 reference genome using STAR aligner, and expression quantification was performed using featureCounts, based on the alignment position and gene definition files. Clustering and differential gene expression analysis were implemented with

iDEP2.01.[33] The resulting *p* values were adjusted for multiple testing using the default method (Benjamini and Hochberg). Adjusted *p* value < 0.05 were analyzed through the use of QIAGEN Ingenuity Pathway Analysis.

Western blot analysis

Cells were harvested and lysed in RIPA buffer (Thermo Fisher Scientific) supplemented with protease inhibitor cocktail and phosphatase inhibitor (Roche, Basel, Switzerland). Lysates were centrifuged at 13,000 × *g* for 15 min at 4°C, and protein concentrations in the supernatants were determined using a bicinchoninic acid (BCA) assay kit (Thermo Fisher Scientific). Equal amounts of total protein (5 μg per lane) were separated by SDS–PAGE on 10–20% polyacrylamide gels and transferred onto Immobilon-P membranes (Millipore). Membranes were blocked with Blocking One (Nacalai Tesque, Kyoto, Japan), incubated with primary antibodies, and signals were detected using the ECL Prime detection kit (Cytiva). Images were acquired using an ImageQuant LAS 4000 system (GE Healthcare). Band intensities were quantified using ImageJ software.

QUANTIFICATION AND STATISTICAL ANALYSIS

Data were analyzed using repeated-measures two-way ANOVA or one-way ANOVA followed by Dunnett's post hoc test, or Student's *t* test, as appropriate, to determine statistical significance. The statistical methods used for each experiment are described in the corresponding figure legends. Differences were considered statistically significant at $p < 0.05$. All analyses were performed using GraphPad Prism software version 9.0 for Windows (GraphPad Software, San Diego, CA).